Ionospheric wave signature of the American solar eclipse on 21 August 2017 in Europe

Tobias G.W. Verhulst*

Stanimir M. Stankov*

Royal Meteorological Institute (RMI), Ringlaan 3, B-1180 Brussels, Belgium

Abstract

A total solar eclipse occurred on 21 August 2017, with the path of totality starting over the North Pacific Ocean, crossing North-America and ending over the Mid-Atlantic Ocean slightly North of the equator. As a result, a partial solar eclipse was observed as far away as the Western Europe. The ionospheric observatory in Dourbes, Belgium, was right on the edge of the partial eclipse and was exposed for a very short period of only few minutes just before the local sunset. High-resolution ionospheric measurements were carried out at the observatory with collocated digital ionosonde and GNSS receivers. The data analysis revealed a clear wave-like pattern in the ionosphere that can be seen arriving before the local onset of the eclipse. The paper details the analysis and provides a possible explanation of the observed phenomenon.

Keywords: Solar eclipse, Digisonde, Ionospheric waves

1. Introduction

A total solar eclipse occurred on 21 August 2017, with a totality path passing through North America and ending in the Atlantic Ocean. The first contact of the penumbra occurred in the North Pacific Ocean at 15:46:52 UT and the last contact was at 21:04:24 UT in the Mid-Atlantic Ocean, close to the equator. The greatest eclipse occurred at 18:25:32 UT at the location with

*Corresponding author

Email address: tobias.verhulst@oma.be (Tobias G.W. Verhulst)

coordinate 36.97°N, 87.67°W, in the USA, where the width of the total eclipse was 114.7 km. Most of the total eclipse path was above North America, ending above the Atlantic Ocean (see Figure 1). As a result, a partial solar eclipse was visible even from Belgium, including the RMI Geophysical Centre in Dourbes (50.1°N, 4.6°E). At this location, the eclipse magnitude was 0.11 with a maximum obscuration of 4.3 %. The eclipse started at 18:41:03 UT (solar zenith angle of 89.7° and azimuth of 288.4°) and ended at 18:48:00 UT, the end coinciding with the local sunset at ground level. However, the sunset at higher altitudes, e.g., at the height of the ionospheric electron density peak hmF_2, happened significantly later. This is due to the shape of the local altitudinal solar terminator, see *Verhulst & Stankov* (2017) for a study on the time variations of sunset with altitude.

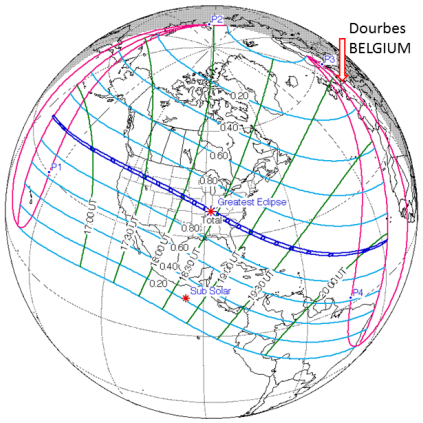

Figure 1: Schematic (credit: NASA) of the solar eclipse on 21 August 2017 at the Earth' surface. The path of the total solar eclipse is denoted by the strip bounded by dark-blue curves, while paths of the partial (0.80, 0.60, 0.40, and 0.20 magnitude) eclipse are plotted with light-blue curves. The progression of the greatest eclipse is marked by green curves with time stamps (UT). The red arrow points at the location of Dourbes, Belgium.

Rapid changes in the solar electromagnetic flux and in the ionising ultraviolet radiation during solar eclipses induce various effects on both the thermosphere and the ionosphere, including modification of the temperature balance and ionisation in the lower ionosphere, as well as of the transport processes in the upper ionosphere, etc. (*Rishbeth*, 1968, 1970). Since the local eclipse at low altitudes above Belgium was within a minute of the sunset at ground level, no major effects of the eclipse were expected to be seen in the lower atmosphere. Given the low obscuration level, no major changes

in the ionospheric plasma density were expected to be produced in the local ionosphere either. However, well known are the wave phenomena generated by the Moon's shadow passing through the atmosphere (*Altadill et al.*, 2001; *Mošna et al.*, 2017). What interested us in this occasion was whether there would be any signs of wave phenomena present in the ionosphere, especially at such a long distance from the totality path. For this purpose, we have set up a high-cadence measurement campaign during the eclipse with ground-based instruments available to us. First results from the solar eclipse of 21 August 2017 are reported here and discussed in view of our previous experience in eclipse observations (*Verhulst et al.*, 2016; *Stankov et al.*, 2017).

2. Instrumentation and measurements

The instruments used in this study are installed at the RMI Geophysical Centre in Dourbes (*Jodogne & Stankov*, 2002). The key instrument is a Lowell Digisonde-4D® (*Reinisch et al.*, 2009), a state-of-the-art equipment using HF radar principles of remote sensing to evaluate, with high accuracy and precision, the conditions of the ionospheric plasma above the station. It is capable of simultaneously measuring the following observables using reflected (in vertical incidence) or refracted (in oblique incidence) signals from the ionosphere: frequency, range, amplitude, phase, Doppler shift and spread, angle of arrival, and wave polarisation. Signal transmission is performed with two (NE-SW and NW-SE) crossed delta antennas of 40 m in height and reception is done with an array of four crossed magnetic dipole antennas in a triangular arrangement. The Digisonde is equipped with the latest version of the computer software for automatic ionogram interpretation, ARTIST-5 (Automatic Real-Time Ionogram Scaler with True height) (*Galkin et al.*, 2008), and Digisonde Drift Analysis, DDA (*Kozlov & Paznukhov*, 2008).

For the purpose of this study, the Digisonde was used to produce ionograms every thirty seconds, the precise settings are listed in Table 1; they are identical to those used during the observation of the 2015 eclipse (*Verhulst et al.*, 2016; *Stankov et al.*, 2017). These settings are optimised to produce, at a high-cadence rate, ionograms of sufficient quality to be scaled easily, but without some less important data. The main differences between the special campaign ionogram configuration and the routine sounding programs are that here only the O-polarised echoes are recorded and not the X-trace, no fine frequency stepping is used, and the 66.7μs pulse wave form is used instead of the 16-chip complementary phase code. This results in shortening

the ionogram runtime to less than fourteen seconds, while the skymap program runs in under thirteen second. Thus, both ionograms and skymaps can be produced at a rate of two per minute.

Table 1: Digisonde program parameters for ionogram and skymap soundings during the August 2017 eclipse campaign (see *LDI* (2009) for more information on Digisonde programming).

	Ionogram	**SkyMap**
Frequencies	1–10 MHz coarse 25 kHz	5 MHz five 50 kHz steps
Polarity	O only	O only
Integrated reps.	4	128
Wave form	$66.\bar{6}\mu s$ pulse	16-Chip comp.
Starting seconds	00 & 30	15 & 45
Sounding time	14.470 s	12.830 s

The ionosonde programs are scheduled in 30-minute batches. At the half hour mark, the self-test and calibration programs are run (*LDI*, 2009). This takes one minute, so every half an hour 58 ionograms can be produced with a one-minute data gap at the half hour mark. This special campaign schedule was run on three days, 20–22 August 2017, between 18:00 UT and 21:00 UT. For all the ionograms produced during this campaign the autoscaled parameters were manually verified and corrected.

On the evening of 20 August, strong sporadic E layers were observed. This made it difficult to correctly scale the important characteristics from the ionograms. Therefore, the observations on the day after the eclipse, 22 August, are used in this study for comparison to those on the day of the eclipse.

TEC observations were carried out with a high-performance GNSS receiver collocated with the Digisonde. The receiver (NovAtel GPStation-6™) can track all present GNSS constellations and satellite signals with a maximum sampling rate of 50 Hz for each of the 120 available tracking channels (*NovAtel*, 2011). The vertical TEC is automatically calculated from the GNSS measurements at an optimal time resolution of 1 minute using the Novatel proprietary software (*Shanmugam et al.*, 2012).

The observations of the previous solar eclipse in 2015 occurred while the ionosphere was recovering from a major geomagnetic storm (*Verhulst et al.*,

2016; *Stankov et al.*, 2017). This is not the case for the 2017 eclipse, since no major storms did occur during the week prior to the event. However, the second half of August 2017 did experience ongoing small disturbances, with the Dst index going down to -32 nT and -30 nT respectively on the days before and after the eclipse. At the same time, the K-like index calculated from the measurements by the local magnetometer in Dourbes (*Stankov et al.*, 2011) shows moderate to active geomagnetic conditions, but never reached storm level values. The day of the eclipse itself was quiet, with the Dst going no lower than -16 nT.

3. Results

Figure 2 shows the evolution of the peak altitude hmF_2 and critical frequency f_oF_2 on the day of the eclipse as well as the day after. The solar terminator, as function of altitude, is also shown. Even though the sunset at ground level happens immediately after the onset of the eclipse, it is clear that sunset at the height of the F_2 peak occurs almost two hours after the eclipse. Therefore, it can be assumed that the sunset is not interfering with the disturbances in the ionosphere caused by the eclipse. The data are shown from 17:00 UT to 21:00 UT for both days, so the first hour comprises data obtained with the routine measurements at five minute intervals, rather than the high cadence campaign soundings.

On the day of the eclipse a wave pattern can clearly be seen in the peak height. This wave has a period of about 25 minutes, and an amplitude of 30–40 km. The wave arrives before the local onset of the eclipse with at least two periods visible between 18:00 UT and 18:40 UT. An earlier period could possibly be fitted to the data starting from 17:30 UT, but because of the lower sounding rate prior to 18:00 UT this can not be confidently ascertained. A final period of the wave can be seen after the local start of the eclipse, ending around 19:15 UT. Some wave-like behaviour can be seen on the day after the eclipse, with more or less constant amplitude throughout the measurement period. This could be a result of the small geomagnetic disturbances observed on the afternoon of this day. The wave patterns seen on both days are qualitatively different: on the day of the eclipse it looks like a short burst of activity, while the waves on the day after persist throughout the period of the campaign. Quantifying these differences is difficult, though, because of the limited period during which high time cadence measurements are available.

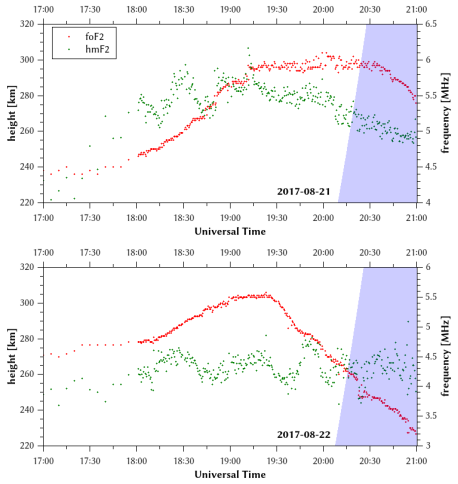

Figure 2: Manually corrected ionospheric characteristics hmF_2 (green) and f_oF_2 (red) at Dourbes on the eclipse day, 21 Aug 2017 (top panel), and the control day, 22 Aug 2017 (bottom panel). The shaded areas on both panels indicate the altitudinal solar terminator.

The critical frequency, and therefore also the peak density, does not exhibit any wave-like behaviour during this period. From around 17:30 UT to 19:30 UT the critical frequency slowly increases from 4.5 MHz to 6 MHz. Only at the moment of the eclipse, at 18:41 UT, a small plateau in f_oF_2 can be observed. However, this is probably an artefact of some incomplete ionograms around this time.

The true-height contours for a range of sounding frequencies are shown in Figure 3, spanning the same period from 17:00 UT to 21:00 UT on both days. The lowest frequency shown is 2 MHz, and it can be seen that at the beginning of the considered time interval, this is below the E-layer critical frequency f_oE. This explains why the contours for the lowest frequencies are flat at 100 km at the beginning of the period. It is evident that during the period of interest the contours for all frequencies are moving in parallel, indicating that the entire ionosphere exhibits a bulk movement. On the control day, some variations in the contours can also be observed. However, close inspections reveals that these are mere fluctuations between subsequent ionograms, rather than systematic movements over a longer time. Hence, these variations cannot be interpreted as waves in the ionosphere. Note that the small plateau in f_oF_2 is not visible here, further indicating that this is just the result of some incomplete ionograms rather than a physical effect of

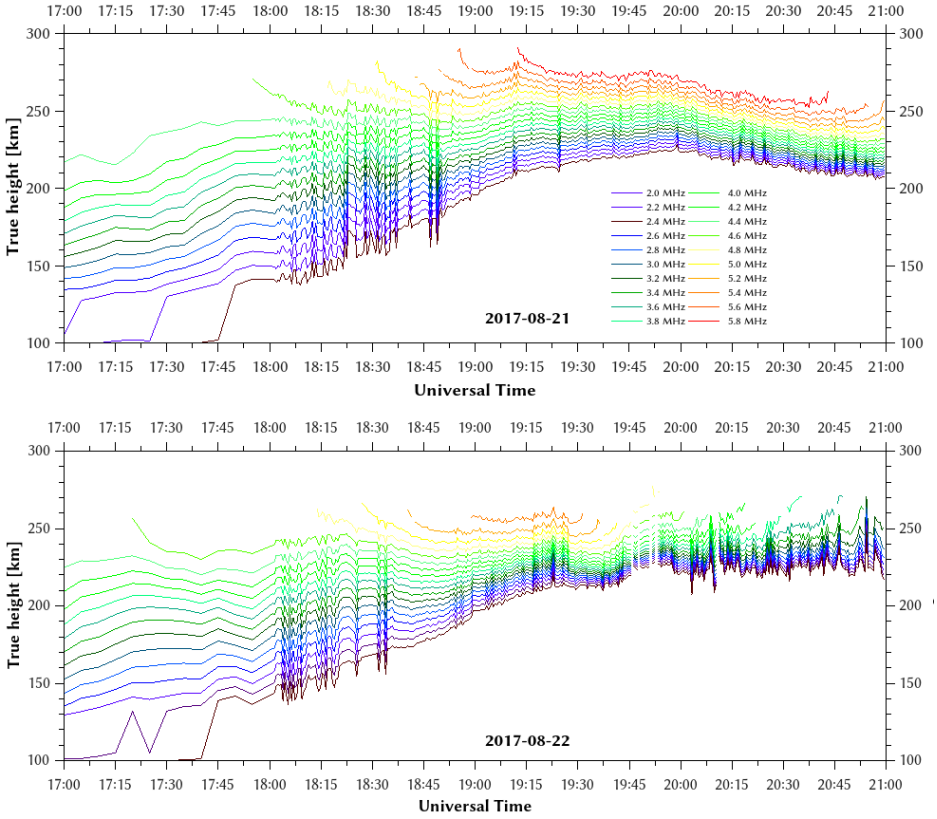

Figure 3: True-height contours for frequencies ranging from 2.0 MHz (bottom curve) up to 5.6 MHz (top curve) in steps of 0.2 MHz as obtained from the ionosonde measurements at Dourbes during the eclipse day (top) and the control day (bottom).

the solar eclipse.

Between 18:00 UT and 21:00 UT, skymap observations were made at the same rate as the ionograms, one sounding every 30 seconds. From these measurements, the drift velocities are calculated using the DDA program (using a five minute smoothing setting, and limiting the used ranges between 150 km and 400 km). Large peaks in the horizontal velocity component v_h can be seen in Figure 4(top panel) coinciding with the peaks observed in the peak height. The direction of these movements is towards the east, and each of the peaks in v_h corresponds to a downward peak in v_z—although the vertical movement is smaller than the horizontal one, as can be seen from the different scales used in Figure 4. This is the expected signature

from a non-acoustic wave in the density. Around the time when the solar terminator crosses the altitude of the F_2 peak, two additional wave features can be observed. They are different in nature, with positive values for both v_h and v_z simultaneously, and are not related to the eclipse but to the solar terminator. The behaviour of both drift components on the day after the eclipse, as seen in the bottom panel of Figure 4. Although some variations with longer periods are visible, e.g. in v_h between 19:30 UT and 20:00 UT, no sharp peaks similar to those observed during the eclipse are present.

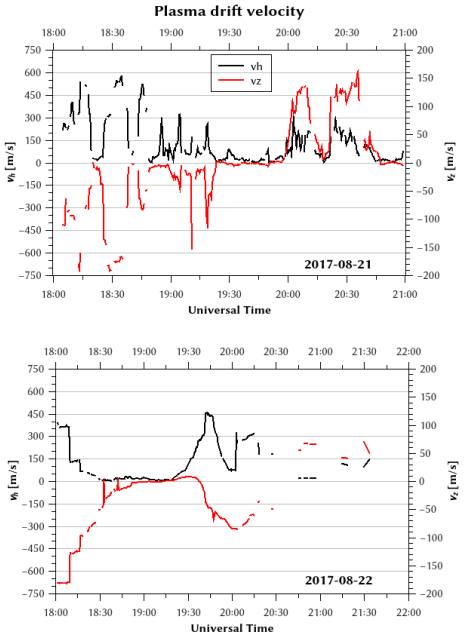

Figure 4: Horizontal (black, left axes) and vertical (red, right axes) components of the bulk plasma velocity on the day of the solar eclipse (top panel) and on the day after the eclipse (bottom panel). Note that both components are plotted on a different scale; in reality the vertical speed is smaller than the horizontal.

Figure 5 shows the vertical total electron content derived from GNSS observations at the Dourbes observatory from 17:00 UT to 21:00 UT, on the day of the eclipse as well as the day after. Very little variability is shown by the $vTEC$ on either day. The main feature in Figure 5 is the slow beginning of the $vTEC$ decrease that is expected around sunset. The $vTEC$ on 22 August is systematically a little lower than on 21 August. This can be explained by the small geomagnetic disturbances on this day, but a further investigation

into this is not in the scope of this paper.

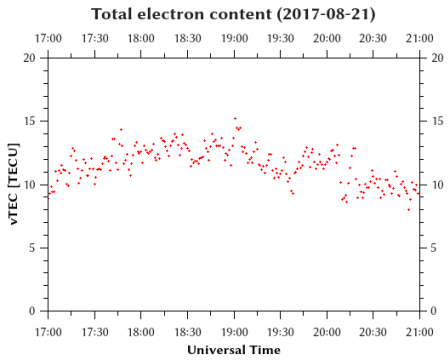

Figure 5: GNSS TEC measurements on 21 (red) and 22 (black) August at Dourbes.

An operational system has been developed and installed at the RMI with the purpose of measuring and displaying the local ionosphere characteristics, including the total electron content, the ionospheric layers' critical frequencies and density peak heights, the plasma scale height, the slab thickness, the ionospheric tilt and plasma drift, etc. LIEDR (Local Ionospheric Electron Density profile Reconstruction) is the main module used for retrieving and processing data in real time from simultaneous GNSS and ionosonde measurements and then constructing the vertical plasma density distribution (profile) in the local ionosphere (*Stankov et al.*, 2011). The resulting full-height ionospheric electron density profile is displayed in the form of a profilogram.

For the period of the solar eclipse observation campaign, the LIEDR model was run at a rate of two profilograms per minute, i.e. a reconstruction of the electron density profile was done for every single ionogram. Since the GNSS derived TEC is only available at one-minute intervals, the same TEC value was reused for two subsequent model runs. During normal operations, the model is used with a height step of 5 or 10 km. However, in order to make sure all variability observed in the peak height is contained in the model, this was set to a 1 km resolution for this campaign. The profilograms produced by the model are shown in Figure 6 (with the electron density converted to plasma frequency). Note that this plot shows the reconstructed profiles between 220 km and 320 km only. This is the region of interest here, even though the model runs for altitudes from 80 km to 1000 km. The output is shown from 17:45 UT until 19:15 UT, were the normal time-resolution of

one ionogram per five minutes was used before 18:00 UT. The gaps at the half-hour marks are the result of missing ionograms due to the house-keeping programs running on the Digisonde—see section 2.

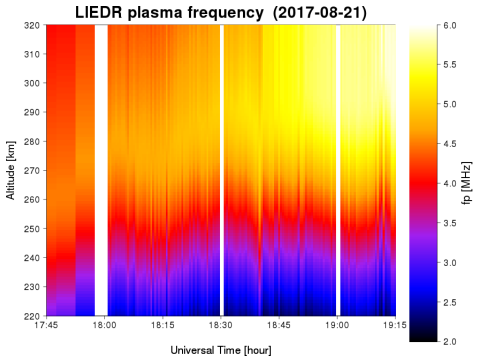

Figure 6: Vertical electron density distribution (converted to plasma frequency in MHz) during the eclipse at Dourbes, as derived by the local ionospheric specification system (LIEDR).

The same wave patterns observed in the true height contour plots (Figure 3) and the peak height hmF_2 (Figure 2) are also evident in the LIEDR profilograms, with two clear, upward motions of the ionosphere around 18:00 UT and 18:30 UT. However, it is clear that the plasma frequency, which corresponds to the peak density NmF_2, does not exhibit any waves but rather a steady increase, as can also be seen from Figure 2.

4. Discussion

Both in the true height contours obtained directly by scaling the ionograms (Figure 3) and in the electron density profiles reconstructed by the LIEDR model (Figure 6), the same oscillations in the altitude of the ionosphere can be observed. This pattern is equally clear from the plot of the peak height hmF_2 (Figure 2). However, no waves are seen in the plot of the peak density. Therefore, the observed disturbance is not an acoustic, as many TIDs are (*Gershman & Grigor'ev*, 1968; *Hocke & Schlegel*, 1996), but rather a vertical movement of the entire ionosphere as a whole. A dedicated campaign to observe the solar eclipse of 20 March 2015 was run at the same location, using the exact same configuration for the ionosonde (*Verhulst et al.*, 2016). These observation gave the same results: waves were detected in hmF_2, true height contours and in the bulk plasma drift, but not in f_oF_2—corresponding

to the peak density—or in the TEC. It is therefore reasonable to assume that the nature of the detected disturbances is the same for both eclipses.

Another peculiar observation is the occurrence of large drifts (deduced from the Digisonde skymap soundings), coinciding with the peaks in hmF_2. In Figure 4(top panel) it can be seen that the vertical component of the bulk plasma drift reaches values as low as 200 m/s downwards. Similar measurements carried out at the same location during the March 2015 solar eclipse, revealed drift values of 60 m/s downwards, but also several distinct peaks of upwards movement (*Verhulst et al.*, 2016). Such upwards movements are entirely absent here. Comparing the top and bottom panels of Figure 4, it can be seen that the bulk plasma drift behave very different on both days. At the time of the eclipse, the extrema in both v_z and v_h can be seen to coincide with the peaks observed in hmF_2 (note that Figure 4 only shows the period during which thirty-second resolution data is available, while Figure 2 shows one more hour before the start of the special campaign). Such a correlation between the different measurements is entirely absent on the day after the eclipse, even though some variations are seen in each parameter separately. The variations seen on 22 August are probably due to some small geomagnetic activity on that day, and the differences between both days point to the very different sources of the disturbances.

During a solar eclipse, the shadow of the moon moves at supersonic speed through the ionosphere. It might therefore seem impossible for waves generated by the eclipse to arrive at the point of observation before the onset of the local eclipse. The early arrival of the waves therefore can be understood if they are generated in a region with a higher obscuration level, with the point of observations being located to the side of the path of the source of disturbances. The observed disturbance is the bow wave produced by the movement of the Moon's shadow through the ionosphere. This is consistent with the large—up to 600 m/s—horizontal component of the bulk plasma drift seen in Figure 4(top panel) being directed towards the East, since the regions of higher obscuration are to the West of the observatory.

During the 2015 event the first waves were not seen to arrive until after the local onset of the eclipse. This is consistent with the hypotheses that the waves are generated at some higher level of obscuration; since the obscuration in Dourbes reached 81.5% during the 2015 eclipse, the observations in that case were made directly on the path of the source of disturbances, rather than to the side of it.

A detailed comparison of the observations during the 2015 and 2017

eclipses is difficult because measurements are only available from a single location for both eclipses. During the 2015 eclipse, the Dourbes observatory was close to the centre of the path of the eclipse while for the 2017 eclipse the observatory is at the very edge of the eclipse path. Thus, during the 2015 eclipse locally originating disturbances were observed, directly related to the decrease in photoionisation above the ionosonde, while during the 2017 eclipse we observed disturbances propagating through the ionosphere from a source closer to the path of totality. A further complication for this comparison is the difference in time of day between the occurrences of both eclipses. The 2015 eclipse reached its maximum at 09:34 UT, which is morning time in Europe, while the effects of the 2017 eclipse were observed in the evening. Therefore, the background condition of the ionosphere was very different for both eclipses.

5. Conclusion

The ionospheric observatory of Dourbes was at the very edge of the path of the solar eclipse of 21 August 2017. Nevertheless, a special campaign of high-cadence ionosonde soundings was run during the eclipse, producing both ionograms and skymaps at a cadence of thirty seconds. No significant disturbances were generated locally by the eclipse, but travelling ionospheric disturbances could be observed moving eastwards over the ionosonde station. These disturbances manifest themselves in the peak height and the true height contours, as well as in the bulk plasma drift. No wave-like variations were observed around the time of the eclipse in the peak density, indicating that the observed wave is a collective vertical movement of the ionospheric plasma, rather than an acoustic wave. These results illustrate the importance of investigating various ionospheric characteristics—peak density and height, TEC, plasma drift velocity—at the same time in order to differentiate between various types of waves and their different possible sources.

The observed waves were, most likely, generated somewhere west of Dourbes where higher obscuration levels were reached. However, with only data from a single ionosonde, it is impossible to determine their exact origin. Although it is possible to detect, for example, the presence of wave phenomena in the ionosphere at a single site, in order to track them and study their evolution with time, high-cadence observations at as many locations as possible along the wave paths are needed. It is evident from the observations presented here that routine measurements at intervals of five minutes provide too coarse a

picture of the time-evolution of the ionosphere to reliably detect this kind of disturbances. Figure 2 illustrates clearly that before the beginning of the high cadence campaign, with the five minute time-resolution, the presence of a wave is difficult to confidently ascertain.

Acknowledgements

This study is supported by the Belgian Solar-Terrestrial Centre of Excellence (STCE).

Altadill, D., Sole, J.G., and Apostolov, E.M. (2001), *Vertical structure of a gravity wave like oscillation in the ionosphere generated by the solar eclipse of August 11, 1999*, J. Geophys. Res. **106**(A10), 21419–21428, doi:10.1029/2001JA900069.

Galkin, I.A., Khmyrov, G.M., Kozlov, A.V., Reinisch, B.W., Huang, X., and Paznukhov, V.V. (2008), *The ARTIST 5* in : P. Song, J.C. Foster, M. Mendillo, and D. Bilitza, (Eds.), *Radio Sounding and Plasma Physics*, AIP Conf. Proc. **974**, 150–159, doi:10.1063/1.2885024.

Gershman, B.N. and Grigor'ev, G.I. (1968), *Traveling ionospheric disturbances—A review*, Radiophys. Quantum El. **11**(1), 5–27, doi:10.1007/BF01033534.

Hocke, K and Schlegel, K. (1996), *A review of atmospheric gravity waves and travelling ionospheric disturbances: 1982-1995*, Ann. Geophys. **14**, 917, doi:10.1007/s00585-996-0917-6.

LDI, Inc. (2009), *Digisonde®4D System Manual* v2.5 (Lowell Digisonde, Lowell, MA).

Jodogne, J.-C. and Stankov, S.M. (2002), *Ionosphere-plasmasphere response to geomagnetic storms studied with the RMI-Dourbes comprehensive database*, Ann. Geophy. **45**(5), 629–647, doi:10.4401/ag-3529.

Kozlov, A.V. and Paznukhov, V.V. (2008), *Digisonde Drift Analysis Software*, AIP Conf. Proc., **974**, 167–174.

Mošna, Z., Boška, J., Koucká-Knížová, P., Šindelářá, T., Kouba, D., Chum, J., Rejfek, L., Potužníková, K., Arika, F., and Toker, C. (2017), *Observation of the solar eclipse of 20 March 2015 at the Pruhonice station*, J. Atmos. Sol.-Terr. Phy. (in press), doi:10.1016/j.jastp.2017.07.011.

NovAtel (2011), *GPStation-6, GNSS Ionospheric Scintillation and TEC Monitoring (GISTM) Receiver User Manual*, OM-20000132.

Reinisch, B.W., Galkin, I.A., and Khmyrov, G.M. (2009), *New Digisonde for research and monitoring applications*, Radio Sci. **44**(1), RS0A24, doi:10.1029/2008RS004115.

Rishbeth, H. (1968), *Solar eclipses and ionospheric theory*, Space Sci. Rev. **8**, 543–554, doi:10.1007/BF00175006.

Rishbeth, H. (1970), *Eclipse effects in the ionosphere*, Nature **226**(5251), 1099–1100, doi:10.1038/2261099a0.

Shanmugam, S., Jones, J., MacAulay, A., and Van Dierendonck, A.J. (2012), *Evolution to modernized GNSS ionospheric scintillation and TEC monitoring*, in: Proc. IEEE/ION PLANS, 24-26 April 2012, Myrtle Beach, SC, USA.

Stankov, S.M., Stegen, K., Muhtarov, P., and Warnant, R. (2011), *Local ionospheric electron density profile reconstruction in real time from simultaneous ground-based GNSS and ionosonde measurements*, Adv. Space Res. **47**(7), 1172–1180, doi:10.1016/j.asr.2010.11.0339.

Stankov, S.M., Stegen, K., and Warnant, R. (2011), *K-type geomagnetic index nowcast with data quality control*, Ann. Geophys. **54**(3), 285–295, doi:10.4401/ag-4655.

Stankov, S.M., Bergeot, N., Berghmans, D., Bolsé, D., Bruyninx, C., Chevalier, J.-M., Clette, F., De Backer, H., De Keyser, J., D'Huys, E., Dominique, M., Lemaire, J.F., Magdalenić, J., Marqué, C., Pereira, N., Pierrard, V., Sapundjiev, D., Seaton, D.B., Stegen, K., Van der Linden, R., Verhulst, T.G.W., and West, M.J. (2017), *Multi-instrument observations of the solar eclipse on 20 March 2015 and its effects on the ionosphere over Belgium and Europe*, J. Space Weather Space Clim. **7**, A19, doi:10.1051/swsc/2017017.

Verhulst, T.G.W., Sapundjiev, D., and Stankov, S.M. (2016), *High-resolution ionospheric observations and modeling over Belgium during the solar eclipse of 20 March 2015 including first results of ionospheric tilt and plasma drift measurements*, Adv. Space Res. **57**(11), 2407–2419, doi:10.1016/j.asr.2016.03.009.

Verhulst, T.G.W. and Stankov, S.M. (2017), *Height-dependent sunrise and sunset: effects and implications of the varying times of occurrence for local ionospheric processes and modelling*, Adv. Space. Res. **60**(8), 1797–1806, doi:10.1016/j.asr.2017.05.042.